Journal of Thermal Engineering
Web page info: https://jten.yildiz.edu.tr
DOI: 10.14744/thermal.0000000

Research Article

# Parametric study and performance evaluation of a multi-layered twin pcm-based vertical thermal energy storage system

**Amit Kumar GHOSH[1,*], Pabitra HALDER[1]**

[1]*Indian Institute of Engineering Science and Technology, Shibpur, 711103, India*

## ARTICLE INFO

*Article history*
Received: 07 March 2024
Revised: 28 June 2024
Accepted: 01 July 2024

**Keywords:**
Alternating Arrangement; Multi-layer; Phase Change Materials (PCMs); Thermal Energy Storage (TES); Twin-PCM

## ABSTRACT

This study illustrates an ingenious approach to thermal energy storage using multi-layer twin-phase change materials (PCMs) alternately arranged inside a vertical shell and tube energy storage system. A complex conjugate heat transfer and fluid flow problem is numerically solved, and the effects of different parameters on energy storage performance are evaluated. This study highlights the impact of the number of layers, radius ratio, and flow Reynolds number in the melting and solidification process of PCMs. It also includes the comparison between multi-layer twin PCMs over single-layer individual PCM. The melting and solidification rate improves approximately by 44.3% and 19%, respectively, as the number of layers ($n$) increases from 2 to 8. Additionally, an 8-layer twin PCM-based system accelerates energy storage and retrieval efficacy, attaining a 33.2% enhancement in stored energy and a 5.3% increase in retrieved energy at a fixed time compared to a 2-layer configuration. It is also observed that in the *8-layer-PCM-1&2* alternating arrangement, the melting rate improved by about 33.65% and 55.84% compared to the *1-layer-PCM-1* and *1-layer-PCM-2* respectively. Similarly, the solidification rate is also promoted in the multi-layer system as compared to the single-layer system. Moreover, it is evident that a lower $R/r$ ratio ($R/r$ = 2) significantly decreases both melting and solidification times by about 78.6% and 89%, respectively, compared to a higher ratio ($R/r$ = 4). Similarly, an increase in the HTF flow Reynolds number correlates with reductions in melting and solidification times by approximately 5.8% and 1%, respectively. This study also facilitates the expedited advancement of both the melting and solidification processes of PCMs with distinct physical justifications that can enable a clear understanding of the improvement of thermal energy storage systems.

**Cite this article as:** Ghosh AK, Halder P. Parametric study and performance evaluation of a multi-layered twin pcm-based vertical thermal energy storage system. J Ther Eng 2025;11(5):1−20.

## INTRODUCTION

Energy is the cornerstone of the entire world as it meets all societal and industrial demands. We are now in a stage where all non-renewable energy resources are almost depleted level. The motivation for the research is going towards the shifting of non-renewable resources to renewable resources. The utilization of some natural resources

***Corresponding author.**
*E-mail address: 2021amp002.amit@students.iiests.ac.in

*This paper was recommended for publication in revised form by Editor-in-Chief Ahmet Selim Dalkılıç*

is less effective because it is sporadic. This sporadicity can be reduced by the utilization of an energy storage unit. The storing medium in this unit is a phase change material (PCM) that is kept inside a sealed, insulated container that can be charged and discharged through a diathermal wall. There are numerous applications, including but not restricted to the following: Latent Heat Thermal Energy Storage (LHTES) [1–4], solar power plants [5,6], solar collectors [7–11], air conditioning and ventilation [12–15], cooling of electronic equipment [16–20], heat recovery thermal management [21–23], and spacecraft [24,25].

In the realm of efficient thermal energy storage, the meticulous selection of phase change materials (PCMs) stands as an important factor, particularly in applications where precise temperature regulation and optimal energy management are imperative. Agyenim et al. [26] conducted a comprehensive review that emphasized the importance of PCM selection in particular applications. In the low to medium temperature range, RT-42 and RT-50 are common types of PCM that are utilized in thermal storage applications [27]. Chaabane et al. [28] investigated the thermal performance of an Integrated Collector Storage Solar Water Heater (ICSSWH) with phase change materials (PCM), such as RT42-graphite. Their findings show that RT42-graphite greatly minimizes night thermal losses, making it a suitable choice for applications for maintaining heat retention overnight is crucial to enhancing overall system performance and efficiency. Cano et al. [29] investigated a thermal storage system based on phase change materials (PCMs) in a homemade heat exchanger. Among the PCMs studied, RT-42 exhibited the highest energy accumulation, indicating higher thermal storage performance and efficient energy transmission. Elbahjaoui and Qarnia [30] examined the thermal behavior of a latent heat storage system (LHSU) integrated with a flat-plate solar collector incorporating various phase change materials (PCMs), such as RT-42, RT-50, and RT-60. The results showed that the quantity of latent heat stored during the charging process was around 19.3 MJ for RT-42, 16.54 MJ for RT-50, and 12.79 MJ for RT-60, with RT-42 having the largest latent heat storage capacity of the three. Şimşek and Demirci [31] compared the melting times of RT-35 and RT-42 in a double-tube concentric heat exchanger using CFD. Their studies showed a significant reduction in melting time, with RT-42 experiencing up to an 86.33% decrease compared to the finless model, surpassing RT-35, which reduced melting time by up to 85%. There is a lot of research that has shown the use of PCM in various thermal energy storage systems. A few studies are listed in Table 1 to show the detailed applications based on different PCMs.

The advent of nano-enhanced phase change materials (nePCMs) has sparked a significant improvement in thermal management and storage systems. In the comprehensive review, Mebarek-Oudina and Chabani [38] highlighted how the integration of nanoparticles into traditional PCMs enhances thermal conductivity while reducing specific heat capacity. This combination produces high thermal diffusivity, which enables nePCMs to store and release heat more effectively. These enhancements considerably increase the performance of thermal storage systems [39], HVAC systems [40], solar systems [41], electrical components [42], and batteries [43]. Several studies that elucidated the advancements and applications of nePCMs in various energy storage systems provide valuable insights into

**Table 1.** Detail review of PCM used for the particular application

| Ref. | PCM | Applications | Contributions |
|---|---|---|---|
| Trp [32] | RT-30 | Vertical Shell and Tube LHTES | Experimental results support numerical desired outcomes by demonstrating non-isothermal paraffin melting and isothermal solidification. |
| Zhang et al. [33] | RT-35 | Vertical Shell and Tube LHTES | Helical fins improve PCM melting in LHTES, resulting in superior thermal performance over traditional designs. |
| Feng et al. [34] | RT-40 | Evacuated solar tube collector | RT-40 considerably improves solar thermal storage, maximizing efficiency and reliability in solar energy systems. remarkably systems that use PCM with a latent heat of 160 kJ/kg perform superior. |
| Alshihmani et al. [35] | RT-35 HC<br>RT-42 | PCB Cooling | The impact of RT-42 and RT-35 HC PCM on PCB cooling, with RT-42 surpassing RT-35 in terms of thermal performance. |
| Refaey et al. [36] | RT-31<br>RT-35<br>RT-42 | Photovoltaic panels | PCM incorporation improves solar panel cooling with RT-42, which uses triangular fins to achieve a 24% temperature decrease while increasing efficiency by 7-8.4%. |
| Xu et al. [37] | RT-42<br>RT-50<br>RT-60 | Horizontal Shell and Tube LHTES | Optimizes triplex-layer PCM melting in LHTES unit using RT-42, RT-50, and RT60 PCMs, considerably lowering melting time by up to 71%. |

**Table 2.** Review of nePCM used for different applications

| Ref. | Applications | Contributions |
|---|---|---|
| Algarni et al. [44] | Tube solar collector | Integrating 0.33 wt% of copper-enhanced phase change materials to an evacuated tube solar collector (ETSC) improves its efficiency by 32%. |
| Bashirpour-Bonab [45] | Multi-tube energy storage | Dispersing 3-7% copper-oxide nanoparticles (CuO) in paraffin RT82 phase-change material (PCM) reduces melting time by 8.07-22.18%. |
| Elarem et al. [46] | Tube solar collector | The addition of 1% Cu nanoparticles to paraffin in an ETSC with fins boosts HTF temperature by 2 K and optimizes PCM melting. |
| Rothan [47] | Cold storage unit | Adding nano-sized particles to water in a finned wavy tank reduced the freezing time by 19.93% for 30-40 nm particles while increasing the freezing rate by 41.16%. |
| Bahrami et al.[15] | Air conditioning ventilating system | Using nano-enhanced PCM wallboards in a room minimizes air-conditioning energy usage by 7.4%, improves energy storage by 4.37%, and reduces fluctuations in temperature by 52%. |
| Zahid et al. [48] | Electronics cooling | NePCM (RT-54HC/$Al_2O_3$) containing 0.25 wt% $Al_2O_3$ nanoparticles reduces base temperature by 36.2%, hence improving electronic device cooling. |
| Swamy et al. [49] | Battery thermal management | Adding 20% CuO and $Al_2O_3$ nanoparticles to PCM raises the melting fraction substantially, increasing thermal uniformity. |

enhancing thermal management and storage performance, as summarized in Table 2.

The heat energy storage and retrieval are carried out considering the melting and solidification of PCM in a cycle. PCM is melted and stored in the thermal energy followed by the retrieval of energy through the solidification processes. The shell-and-tube design stands as a widely preferred configuration employed in latent heat thermal energy storage (LHTES) systems, where PCMs are utilized to absorb and release heat energy. The storage performance of shell-and-tube LHTES systems can be improved through various design modifications. Cao and Faghri [50] studied the effect of geometrical factors viz. Length to diameter ratio ($L/D$), radius ratio ($r_0/D$) considering a horizontal type storage system. This numerical study demonstrated a slight decrease in energy storage density with the $L/D$ ratio and a significant reduction with $r_0/D$. Ismail and Melo [51] investigated a vertical energy storage unit and established a correlation between heat transfer rate and solidification time. The findings revealed that melting time increased with an increase in $H/r_0$and $R_0/r_0$. Trp et al. [52] explored the impact of $L/D$ and $r_0/D$ on both melting and solidification considering a vertical storage. The findings showed that the selection of geometrical parameters had a substantial impact on the rate of heat transfer and the amount of energy stored or released. Tao et al. [53] studied on horizontal LHTES system that shows the time taken for melting increased by 16.3% when the outer radius expanded from 24.0 mm to 28.0 mm, whereas it decreased by 45.4% when the velocity increased within the range of 10 - 20 m/s. The effect of eccentricity concerning the inner and outer tube was explored by Zheng et al. [54] to analyze melting and melting-solidifying characteristics. It also highlighted the consequences of the Rayleigh number on the optimum eccentricities. Shen et al. [55] studied two different configurations altering the shell radius while maintaining a fixed HTF-tube radius and varying the HTF-tube radius while keeping the outer PCM shell radius constant. The study revealed that the density of energy storage/retrieval was optimal at a radius ratio of 5.

It is essential to take into account the LHTES system's performance with different geometrical configurations. Vyshak et al. [56] compared the melting rates of PCM filled in cylindrical, rectangular, and cylindrical shell containers with equal heat transfer area and volume. It was observed that the melting duration was shortest for PCM stored in a cylindrical shell container, with a noticeable impact of the PCM mass increase on its geometry. Akgun et al. [57] evaluated the results of conical and non-conical storage in terms of melting time and came to the conclusion that conical storage reduced melting time by 20%. A comparative study between conical and cylindrical shell-type storage systems was conducted by Seddegh et al. [58]. It revealed that while the solidification time was nearly the same, the conical tube-shaped unit melted 12% faster than its cylindrical counterpart. Alaraji et al. [59] investigated the melting and solidification characteristics of RT-26 in an LHTES system with an elliptic inner tube. It was revealed that the time for complete melting deteriorated with an increment of the eccentricity of the inner tube. An annular tube comprising vertical and horizontal heat storage was the subject of an experimental study by Dukhan et al. [60]. This study shows how the orientation of storage units has a major effect on the charging of PCM. This was concluded that vertical-type heat exchangers can store more energy than horizontal. Zağlanmiş et al. [61] investigated numerically

a thermal storage system based on several pipe sequences developed for body-pipe-type heat exchanger models. The findings reveal that the duration of melting deteriorates with the increment of HTF inlet temperature. It was also observed that the sequence of the tube affects the melting rate and stored energy.

Another popular method for improving heat transfer is to place extended additional surfaces like fins inside the PCM and a heat source/sink. The main advantage of using a fin is it increases the surface area that resulting in uniform heat transfer which expedites the phase transition process. Paria et al. [62] experimented on a horizontal LHTES system with annular fins of 24 and 48 numbers. They showed that charging time decreased by 58% and 76% in two different cases. Joshi and Rathod [63] studied LHTES systems using fin. It was obtained that the optimal location and size of the fin reduce the melting time. They have used a fin design that enhances the thermal performance than conventional fin configuration at about 4.38%. Nakhchi and Esfahani [64] increased the efficacy of a vertical LHTES system by adopting a new design of upward and downward-stepped fins. It was observed that all stepped fin configurations outperformed straight fins in terms of thermal performance. To assess the impact of the length and fin number that are positioned radially on the functionality of a horizontally oriented cylindrical LHTES system, Nie et al. [65] showed a numerical study using a 2D axisymmetric domain. The melting was found to be enhanced more quickly by the straight fins than by the angled, lower, and upper fin configurations. Nóbrega et al. [66] explored the impacts of axial fins that are positioned vertically along a central pipe in a cylindrical LHTES system. It was observed that the entire solidification time decreased as the number and width of the fins increased. Tiari et al. [67] studied the numerical investigation of the LHTES system using six different annular fin configurations. The twenty-fin arrangement with a constant length was proven to be the most effective arrangement in terms of both melting and solidification time, which reduced the overall time by approximately 76.3%.

In recent years, the multi-layered arrangement is one of the novel approaches in which single or multiple PCMs are arranged in layers. Brousseau and Lacroix [68] studied the thermal performance in a multi-layered system that aimed to reduce the energy load during a peak demand period. The output heat load and the total energy stored were proposed to be correlated as a function of the design factors and operating conditions. Li et al. [69] investigated an LHTES unit in which three PCM were considered. They compared the melting rate of three PCMs and suggested the optimum length for three PCMs. Ezra et al. [70] examined different rows of PCMs arranged in cascaded manners. It was determined for the number of different materials what range of melting temperatures would result in the fastest melting. Beemkumar et al. [71] experimented to explore the heat transfer of cascaded energy storage considering multiple types of fins. It was found that the copper-encapsulated annular finned balls with D-mannitol as the PCM had a faster rate of energy transfer both during charging and discharging. Prasad et al. [72] conducted a comparative study on three PCM-based cascaded LHTES units. The comparison of the combined model with the model solely based on conduction demonstrated that the pure conduction model underestimates the rate of heat transfer between the HTF and PCM at lower flow velocities of the HTF, where free convection significantly influences the phase change phenomena. Kareem et al. [73] investigated a multi-slab latent heat storage system in which nine slabs are filled with RT-25 and RT-21. The results demonstrated that the height of the channel, the height of the PCM slab, the melting temperature of PCM, and the length-to-width ratio strongly affect the melting and solidification performance.

This work introduces an advanced approach to thermal energy storage that uses a multi-layer twin PCM-based vertical thermal energy storage system with an alternating PCM arrangement. As per the authors' knowledge, previous studies have mainly explored the use of uniform PCM layers. This study investigates the effectiveness of using two PCMs with different melting temperatures arranged alternately, a configuration that has not yet been examined. Its unique configuration is intended to increase both energy storage density and retrieval speed. The number of layers, radius ratio, and Reynolds numbers of the HTF flow are investigated to determine their impact on system performance. By comparing single and multi-layer configurations, the study elucidates PCM melting and solidification processes and their impact on energy storage performances. The results demonstrate that the alternating PCM arrangement significantly improves the melting and solidification performances, leading to more efficient energy storage and faster energy recovery. These findings have promising implications for a wide range of thermal storage applications, including renewable energy systems, backup power solutions, thermal management in electronics, building temperature regulation, industrial waste heat recovery, and transportation systems like electric vehicles and aerospace.

## PHYSICAL MODEL

A two-dimensional vertical axisymmetric model as depicted in Figure 1, has been considered in the present computation. The domain consists of a tube surrounded by a shell of multi-layered twin-phase change materials arranged in alternating fashion. Each PCM layer is separated by a thin thermally coupled wall. Each layer is divided in such a way that both PCMs have the same mass. The outer surface of the shell and the extended tube are maintained in thermally insulated condition. The tube radius ($r$), shell length ($L_s$) and tube length ($L_t$) are considered as 12.5 mm, 500 mm, and 700 mm respectively. The radius of the shell ($R$) has been varied based on the radius ratio ($R/r$) 2, 3, and 4. The number of layers ($n$) of PCM ranges

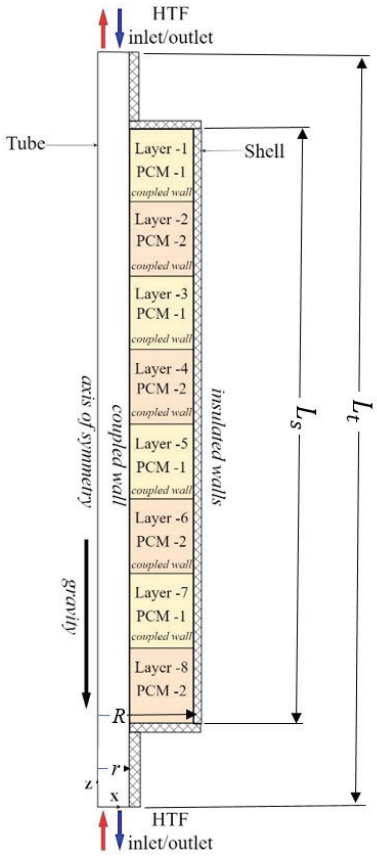


**Figure 1.** Schematic diagram of the physical model.

between 2, 4, and 8, with each layer having equal length. There are three velocity inlet conditions are selected based on Reynolds number (*Re*) of 5000, 10000, and 15000.

During the melting of PCMs, hot heat transfer fluid at 80 °C flows in the upward direction and charges the PCMs. The initial temperature of PCMs is kept at 25 °C. Whereas in solidification, the reverse process is executed. During the solidification, the cold HTF at 25 °C flows in the downward direction and discharges the PCMs. The thermophysical properties of PCM-1, PCM-2, and HTF are tabularized in Table 3.

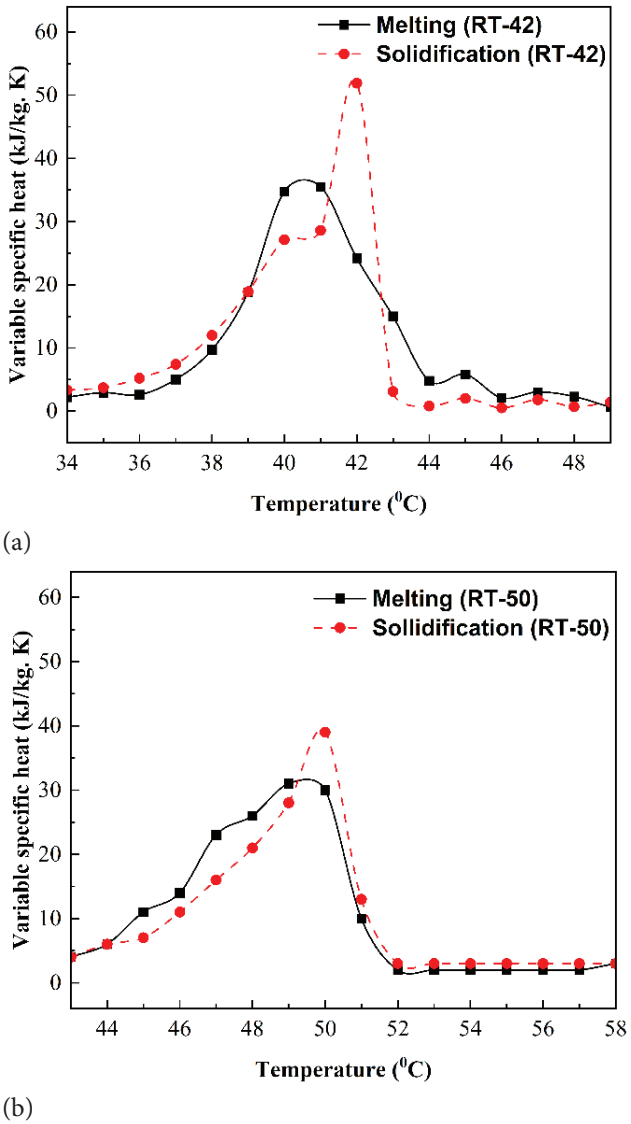


**Figure 2.** Variable specific heat with the temperature of (a) PCM-1 (RT-42) and (b) PCM-2 (RT-50).

**Table 3.** Thermo-physical properties of PCM-1, PCM-2, and HTF [60] [74]

| Description | PCM-1 (RT-42) | PCM-2 (RT-50) | HTF (water) |
|---|---|---|---|
| Density (solid/liquid), (kg/m$^3$) | 880/760 | 880/760 | 998.2 |
| Specific heat, (kJ/kg K) | variable (Fig. 2) | variable (Fig. 2) | 4.182 |
| Thermal Conductivity, (W/m K) | 0.2 | 0.2 | 0.6 |
| Dynamic viscosity, (kg/m s) | 0.0030 | 0.0038 | 0.001003 |
| Thermal expansion coefficient, (1/K) | 0.0008 | 0.0006 | - |
| Latent heat of fusion, (kJ/kg) | 165 | 160 | 335 |
| Solidous temperature, (°C) | 38 | 45 | 0 |
| Liquidous temperature, (°C) | 42 | 50 | 0 |

## MATHEMATICAL MODEL AND BOUNDARY CONDITION

A 2D model is considered to examine the transient heat transfer, fluid flow, and melting and solidification processes. For the simplicity of present numerical computation, a few assumptions have been made: (i) HTF and liquid PCMs are incompressible, (ii) viscous dissipation and radiation heat exchange are neglected, (iii) thickness of solid boundaries are neglected, (iv) PCMs volume expansions are neglected. The coupled non-linear differential equation has been solved for HTF as well as PCMs [55].

### *Mathematical Modeling for HTF*

The conservation of mass is stated by

$$\rho_{HTF}\,(\nabla \cdot \vec{V}_{HTF}) = 0 \tag{1}$$

The conservation of momentum and energy is expressed below:

$$\rho_{HTF}\frac{\partial}{\partial t}(\vec{V}_{HTF}) + \rho_{HTF}\nabla\cdot(\vec{V}_{HTF}\vec{V}_{HTF}) = \nabla\cdot\left((\mu_{HTF}+\mu_{t,HTF})\nabla\vec{V}_{HTF}\right) + \rho_{HTF}g - \nabla p_{HTF} \tag{2}$$

$$\frac{\partial(\rho_{HTF}C_{p,HTF}T_{HTF})}{\partial t} + \nabla\left(\vec{V}_{HTF}(p_{HTF}+\rho_{HTF}C_{p,HTF}T_{HTF})\right) = \nabla\cdot\left((K_{HTF}+K_{t,HTF})\nabla T_{HTF}\right) \tag{3}$$

Where, $\mu_{t,HTF}$ and $K_{t,HTF}$ are viscosity and thermal conductivity due to turbulence are as follows:

$$\mu_{t,HTF} = C_{\mu}\rho_{HTF}\frac{k^2}{\varepsilon} \tag{4}$$

$$K_{t,HTF} = \frac{\mu_{t,HTF}C_{p,HTF}}{Pr_{t,HTF}} \tag{5}$$

Here, $k$ and $\varepsilon$ are the turbulent K.E and rate of dissipation respectively. $k$ and $\varepsilon$ can be evaluated considering the standard $k$-$\varepsilon$ turbulent modeling which is governed by the following equation:

$$\frac{\partial(\rho_{HTF}\,k)}{\partial t} + \nabla.\left(\rho_{HTF}\vec{V}_{HTF}k\right) = \nabla.\left(\mu_{HTF}+\frac{\mu_{t,HTF}}{\sigma_k}\nabla k\right) + G_{k,HTF} + G_{b,HTF} - \rho_{HTF}\varepsilon \tag{6}$$

$$\frac{\partial(\rho_{HTF}\,\varepsilon)}{\partial t} + \nabla.\left(\rho_{HTF}\vec{V}_{HTF}\varepsilon\right) = \nabla.\left(\mu_{HTF}+\frac{\mu_{t,HTF}}{\sigma_\varepsilon}\nabla\varepsilon\right) + \frac{\varepsilon}{k}\left(C_1G_{k,HTF} - C_2\rho_{HTF}\varepsilon\right) \tag{7}$$

Where, $G_{k,HTF}$, $G_{b,HTF}$ is turbulent K.E. generation due to velocity gradient and buoyancy respectively. The values of $C_{\mu}$, $C_1$, $C_2$, $Pr_{t,HTF}$, $\sigma_k$, $\sigma_\varepsilon$ are 0.09, 1.44, 1.92, 0.85, 1.0, and 1.3 respectively.

### *Mathematical Modeling For Pcm*

Enthalpy-porosity method is employed to model the solid-liquid phase transition process. The model consists of the conservation of mass, momentum, and energy which are as follows:

$$\rho_{PCM}(\nabla\cdot\vec{V}_{PCM}) = 0 \tag{8}$$

$$\rho_{PCM}\left(\frac{\partial}{\partial t}(\vec{V}_{PCM}) + \nabla\cdot(\vec{V}_{PCM}\vec{V}_{PCM})\right) = \nabla\cdot\left(\mu_{PCM}\nabla(\vec{V}_{PCM})\right) + \rho_{PCM}\left(1-\beta(T-T_{ref})\right)g - \nabla p_{PCM} + \overrightarrow{S_\gamma} \tag{9}$$

$$\frac{\partial(\rho_{PCM}h_{PCM})}{\partial t} + \nabla\cdot\left(\rho_{PCM}\vec{V}_{PCM}h_{PCM}\right) = \nabla\cdot\left(K_{PCM}\nabla(T_{PCM})\right) \tag{10}$$

Here, $\mu_{PCM}$ and $p_{PCM}$, $\vec{V}_{PCM}$ are PCM's dynamic viscosity, static pressure, and velocity respectively. The variation of density in the buoyant force part in the momentum equation is taken as the Boussinesq approximation to account for the free convection flow phenomenon. The extra source term $\overrightarrow{S_\gamma}$ is the momentum sink term which is represented as follows

$$\overrightarrow{S_\gamma} = C_{mush}\,\frac{(1-\gamma)^2}{\gamma^3+\delta}\vec{V}_{PCM} \tag{11}$$

$$\gamma = \begin{cases} 0, & T \leqslant T_{PCM,\,S} \\ \dfrac{T-T_{PCM,\,S}}{T_{PCM,\,L}-T_{PCM,S}}, & T_{PCM,S} < T < T_{PCM,\,L} \\ 1, & T \geqslant T_{PCM,\,L} \end{cases} \tag{12}$$

Where, $C_{\text{mush}}$ is a constant, called the mushy zone constant. In the current study, $C_{\text{mush}}$ is kept as a default value of $10^5$ kg/ m$^3$. s. Here, $\delta$ is a small constant considered to prevent zero division when the PCM is completely solid and the melting process is starting., i.e., liquid fraction, $\gamma = 0$.

The volumetric enthalpy, $h_P$ the energy equation is stated below:

$$h_{PCM} = h_{ref} + \int_{T_{ref}}^{T} C_{p,v}dT + \gamma L \tag{13}$$

Where, $h_{ref}$ is the reference PCM enthalpy estimated at $T_{ref}$ and $L$ is the latent heat of the fusion of PCM. The energy stored and recovered during charging and discharging is evaluated by

$$Q_T = \frac{Q(t)}{m_{PCM}} \tag{14}$$

$Q(t)$ and $m_{PCM}$ are the energy stored at time instance t and the mass of PCM respectively. $Q(t) = H - H_{Ref}$, $H_{Ref}$ is the reference enthalpy at the reference temperature, and $H$ can be calculated as follows:

$$H = \int_0^V h_{PCM}\rho_{PCM}dV \tag{15}$$

### *Mathematical Modeling for Thermally Coupled Walls*

$$\rho_{wall}\frac{\partial}{\partial t}(h_{wall}) = K_{wall}\nabla\cdot(\nabla T_{wall}) \quad (16)$$

Where, $h_{wall}$ and $K_{wall}$ are the enthalpy and thermal conductivity of the thermally coupled wall. $h_{wall}$ is calculated by the following integral.

$$h_{wall} = \int_{T_{ref}}^{T_{wall}} C_{p,wall}dT \quad (17)$$

***Boundary and Initial Conditions***

Boundary and initial conditions are selected as follows:

HTF inlet: (i) Velocity inlet boundary condition, $V_x = 0$, $V_z = V_{inlet}$,

(ii) $T_{HTF} = T_{inlet} =$ 80 °C / 25 °C (melting/solidification)

HTF outlet: Outflow boundary condition

PCM: $T_{PCM} = T_{int} =$ 25 °C / 80 °C (melting/solidification)

Thermally coupled wall : (i) $V_x = 0$, $V_z = 0$ (ii) wall adjacent to tube, $K_{wall}\frac{\partial T_{wall}}{\partial x} = K_{HTF}\frac{\partial T_{HTF}}{\partial x}$, (iii) wall adjacent to PCM, $K_{wall}\frac{\partial T_{wall}}{\partial x} = K_{PCM}\frac{\partial T_{PCM}}{\partial x}$, (iv) walls in-between layers, $K_{wall}\frac{\partial T_{wall}}{\partial z} = K_{PCM}\frac{\partial T_{PCM}}{\partial z}$

Insulated walls: (i) $V_x = 0$, $V_z = 0$ (ii) $\frac{\partial T}{\partial x} = 0$, $\frac{\partial T}{\partial z} = 0$

## NUMERICAL METHODOLOGY AND VALIDATION

All the non-linear governing equations are numerically computed in the Finite Volume Method (FVM) based commercially available software package ANSYS Fluent 2019 R3. The advantages and flow chart of FVM are elucidated in the appendix section. The solid-liquid phase change process is modeled using the enthalpy-porosity technique [75]. The solver adopts an enthalpy-porosity formulation, considering the liquid-solid mushy zone as a porous medium with porosity equal to the liquid fraction, and includes a momentum sink term in the momentum equations to account for pressure drop caused by solid material. The coupled algorithm is considered to combine the pressure correction and velocity for solving continuity and pressure field. Pressure correction is accomplished by the PRESTO scheme. The Second-Order Upwind discretization is selected to attain higher-order accuracy at cell face values in momentum, energy, turbulent kinetic energy, and dissipation rate equations. The gradient between two cell values is calculated by the Least Squares Cell-Based scheme. The transient formulations are accomplished by the First Order Implicit scheme. The under-relaxation factors for momentum, energy, liquid fraction, turbulent kinetic energy, and turbulent dissipation rate are 0.75, 1, 0.9, 0.8, and 0.8 respectively. The criteria for convergence are set at $10^{-06}$ for continuity, momentum, turbulent K.E, and turbulent dissipation rate whereas $10^{-09}$ is selected for the energy equation. The identical solution methodology is employed for both the melting and solidification processes due to their inherent inversion. The computation facility used for simulation is Intel® Xeon® CPU E5-2650 v3 @ 2.30GHz.

For checking the consistency of the present numerical model, computational outcomes are verified with experimental results. Figure 3(a), illustrates the variation of the liquid fraction with flow time at three different HTF inlet temperatures which is experimented with by Dukhan et al. [60]. The present results show a very good match with the experimental results. This validation model is replicated in all the simulations to achieve good accuracy and closer results to the experimental. A secondary validation is performed to ensure the accuracy of the present FVM code by comparing it with previously reported numerical findings. This verification is accomplished by comparing the current

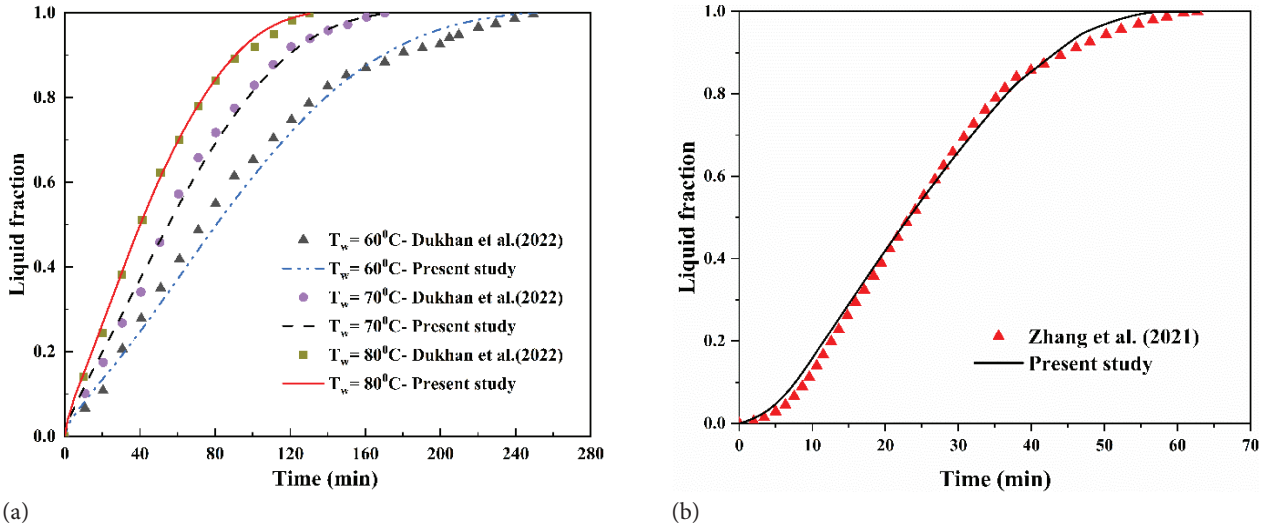


(a) (b)

**Figure 3.** Verification of present numerical results with (a) experimental data, (b) numerical simulation data.

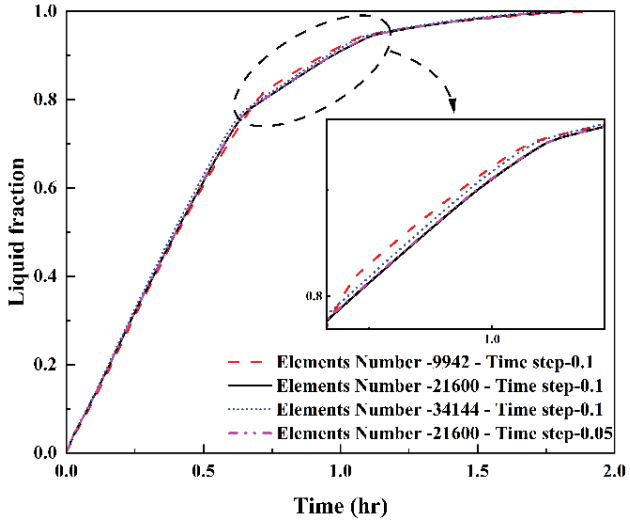


**Figure 4.** Grid and time independence test.

numerical predictions with the numerical results reported by Zhang et al. [76] in Figure 3(b).

## GRID AND TIME INDEPENDENCE TEST

Grid independence test is performed by considering different element numbers as depicted in Figure 4. It is understood that results are almost constant beyond 21600 number elements. We fixed the number of elements to 21600 and checked for the time independence test. It is seen that beyond the elements 21600 and time step of 0.1s there is very negligible change in the liquid fraction. So, in all the simulations the number of elements is considered as 21600, and the time step of 0.1s. It is also to be noted here that the same number of elements and the time step are used in the validation study for achieving good accuracy with the experimental and numerical.

## RESULTS AND DISCUSSION

### During Melting of PCM

Figure 5a depicts the temporal variation of the liquid fraction with the number of layers of PCMs during the melting process. As the number of layers ($n$) varies from 2 to 8, the overall liquid fraction has a significant change. The time needed for fully melting is shortened by 44.3% if the number of layers ($n$) is increased from 2 to 8. When the number of layers is 2, PCM-1 and PCM-2 are separated by a single thermally coupled wall. Initially, both layers have an initial temperature lower than the melting point of both PCM. The melting process begins near the tube wall surface, spreading into PCM-1 and PCM-2. Figure 6 presents the contours of the liquid fraction and temperature. It is seen that PCM-1 melts faster than PCM-2. This is because the PCM-1 with a lower melting point will start to melt at a lower temperature and use less heat energy to reach that temperature. As soon as the PCM-1 begins to melt, it may absorb heat energy more quickly and distribute it faster throughout its entire volume than the PCM-2.In Figures 7a and 7b, it can be observed that a clockwise vortex is formed in the melted pool of both PCM-1 and PCM-2. This represents the natural convection currents driven by temperature gradients within both PCMs. As the PCMs absorb heat, they change from solid to liquid, creating regions of varying density. The melted PCMs near the heat source become less dense and rise, while the cooler, denser liquid descends, resulting in convection currents. The intensity of the vortex near the melt front is greater in PCM-1 than in PCM-2. This indicates that PCM-1 has stronger convection currents than PCM-2, which increases heat transfer rates and accelerates the melting process. The stronger nature of the vortex in PCM-1 facilitates more efficient mixing and heat distribution throughout the melted zone, resulting in a faster-moving melt front. From the temperature contours, it is also observed that there exists a temperature gradient between layers that derives heat flow through the thermally coupled walls, both conductively and convectively. This promotes consistent heat distribution and speeds up the overall melting rate, emphasizing the synergistic effect of temperature gradients and thermally coupled walls in multi-layered PCM systems. It can also be seen from Figure 7d that the vortex near the melt front in PCM-1 disappears, but in Figure 7a, the vortex near the melt front in PCM-1 is evident. It is also obvious that more melting volume is seen inside the melt pool in the case of 8 layers than 2 layers. More melts mean a larger volume of fluid, which may be enough to disrupt the vortex and create a more stable flow pattern. When the number of layers is 8, PCM-1 and PCM-2 are alternately arranged and each of the layers is separated by a thermally coupled wall, a temperature gradient in between layers is created that leads to differences in density within the PCMs, driving natural convection currents where warmer, less dense fluid rises and cooler, denser fluid sinks. However, the presence of thermally coupled walls and alternating PCM materials introduces a more complex flow pattern. Specifically, at the junctions between different PCM layers, the interaction of opposing thermal and fluid flow fields from each layer leads to the formation of counter-rotating vortices. From Figure 7b and 7c, it can be seen those temperature-induced counter-rotating vortices formed near the conjunction of two PCM layers. Those vortices create a low-pressure region at the center. This can cause the melted PCMs to be drawn in from the surrounding region, increasing fluid mixing and promoting convective heat circulation. It can be noticed that the strength and intensity of the vortices increase as the number of layers increases. Figure 7c shows multi-counter rotating vortices formed near the conjunction between two layers. It is evident in proper mixing that accelerates the heat transfer which causes a high liquid fraction as flow time marched.

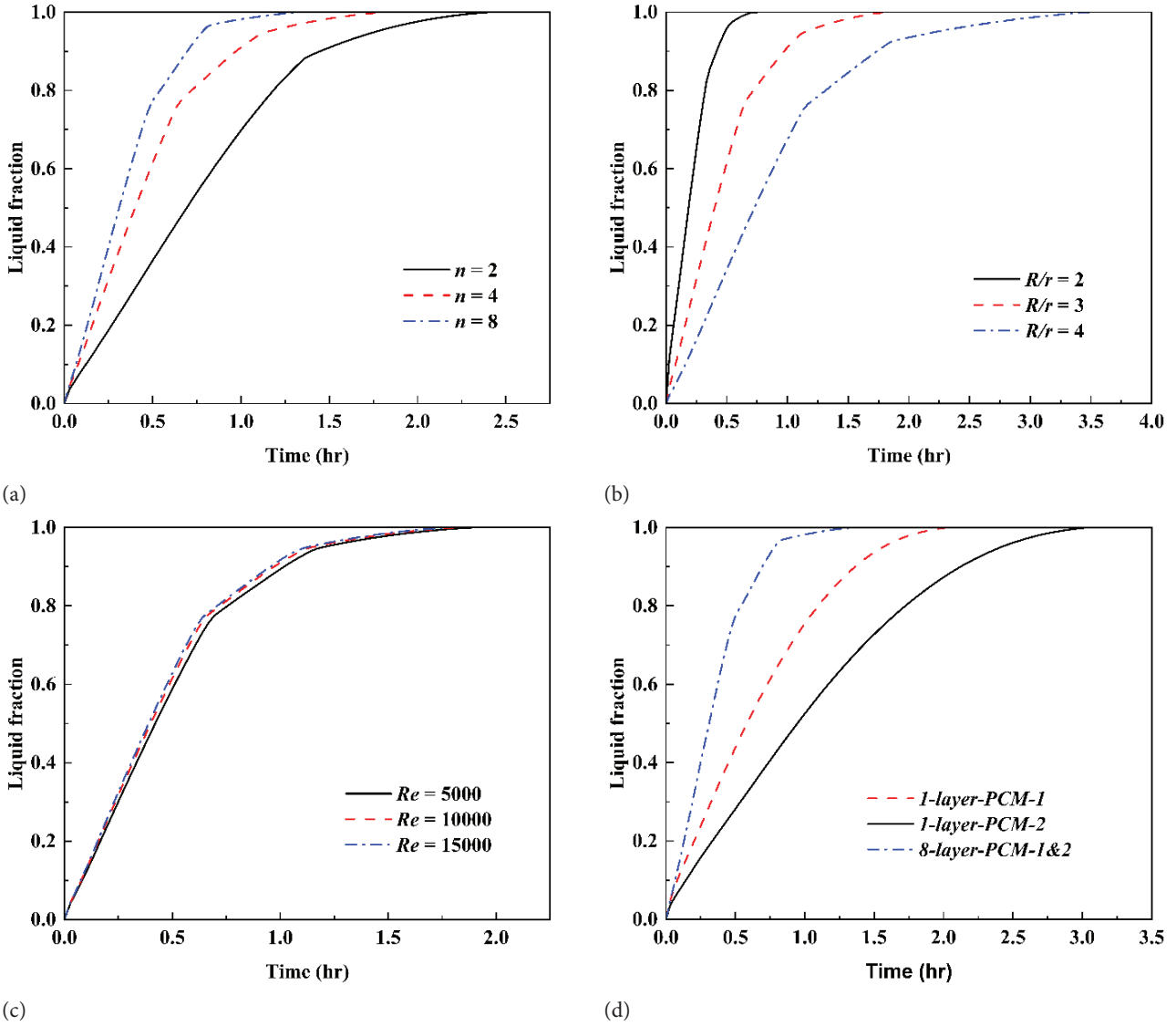


**Figure 5.** Temporal variation of liquid fraction with different parameters during melting of PCMs at (a) $Re$ = 10000, $R/r$ = 3, (b) $Re$ = 10000, $n$ = 4, (c) $n$ = 4, $R/r$ = 3, (d) $Re$ = 10000, $R/r$ = 3.

Figure 5b illustrates the variation of liquid fraction with the radius ratio of shell and tube. It can be observed that raising the $R/r$ ratio and keeping the tube ratio constant leads to an increase in melting time. Specifically, lowering the $R/r$ ratio from 4 to 2 decreases the time needed for complete melting by 78.6%. This phenomenon results from the interaction between thermal mass and thermal resistance. As the shell radius increases, so does the volume and mass of the PCMs within it, necessitating more thermal energy to reach the melting point and resulting in increased thermal inertia. This increased mass introduces more thermal resistance, decreasing total heat transfer and hindering the rate at which the PCM's average temperature rises. Furthermore, the increased shell radius necessitates heat to traverse a greater distance from the tube to the outer shell, thereby augmenting thermal resistance and prolonging the melting duration. Conversely, a lower $R/r$ ratio decreases the PCM volume, reducing both thermal mass and thermal resistance, thus allowing quicker heat transfer and accelerating the melting process. However, this also leads to a lower thermal storage capacity due to less material available for energy storage. Therefore, while designing a thermal energy storage system, the radius ratio of the shell to the tube must be taken into account, as it has an important impact on melting time and overall performance. To ensure a reasonable trade-off between quick melting and sufficient thermal storage capacity, balancing the $R/r$ ratio is essential for maximizing system performance.

Figure 5c describes the variation of the liquid fraction at different HTF flow Reynolds numbers. It is seen that liquid fraction improves with HTF flow Reynolds number. Quantitatively rise in Reynolds number ($Re$) from

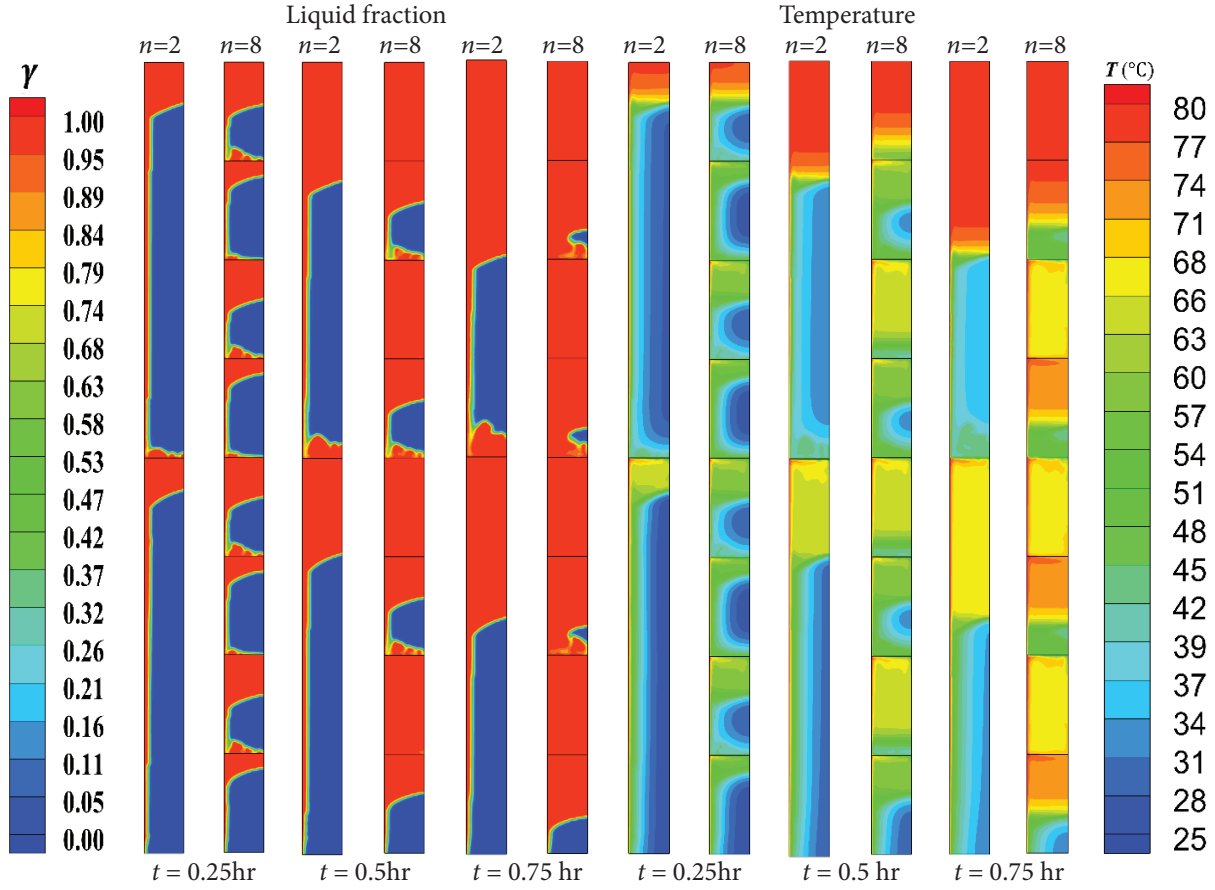


**Figure 6.** Contours of liquid fraction and temperature at different flow times and number of layers during melting of PCMs at $Re$ = 10000, $R/r$ = 3.

5000 to 15000 can reduce the melting time by about 5.8%. Convective heat transfer has been improved, which can account for the rise in the liquid fraction that occurs as the Reynolds number rises. The turbulent nature of the fluid flow that results from a rise in the Reynolds number might result in a greater heat transfer coefficient between the HTF and PCMs. The larger liquid fraction that emerges from the enhanced heat transfer coefficient can be attributed to the increased amount of heat that is transmitted from the HTF to the solid PCMs. However, the enhancement in liquid fraction with an increase in the Reynolds number is typically small because the heat is transferred from the HTF to the solid PCMs through a process called conduction. Nevertheless, compared to the rate at which heat may move through the HTF, the solid PCM normally conducts heat at a significantly slower rate. This is because PCMs are often significantly less thermally conductive than HTF, which makes them less effective in transferring heat. Hence, when PCMs are heated by the HTF, heat may accumulate inside the solid PCMs more quickly than it can be transmitted out from the heated region. This can lead to a temperature gradient within the PCMs, with the heated region having a higher temperature than the surrounding PCMs. If the temperature of the heated region reaches the melting temperature of the PCMs, the PCMs will begin to melt. However, the rate at which the PCMs melt will be limited by the rate at which heat can be conducted away from the heated region. In other words, the solid PCMs will act as a thermal bottleneck that limits the overall melting rate. This bottleneck effect arises due to the thermal resistance encountered within solid PCMs, impeding the heat flow from hotter to cooler regions, thus delaying the phase change process. Therefore, even if the flow rate of the HTF is increased, the overall melting rate may not increase significantly if the solid PCMs act as a thermal bottleneck. In this case, the rate of heat transport through the PCMs will continue to limit the melting rate, regardless of the flow rate of the HTF.

Figure 5d explains the comparison of time variation of the liquid fraction with three different cases viz. *1-layer-PCM-1*, *1-layer-PCM-2*, and *8-layer-PCM-1&2* alternating arrangement. The finding itself provides a better understanding of the selection of the multi-layer configuration. The overall melting time is reduced in the eight-layered configuration by 33.65% and 55.84% as compared to the single-layer of PCM-1 and PCM-2 respectively. Firstly,

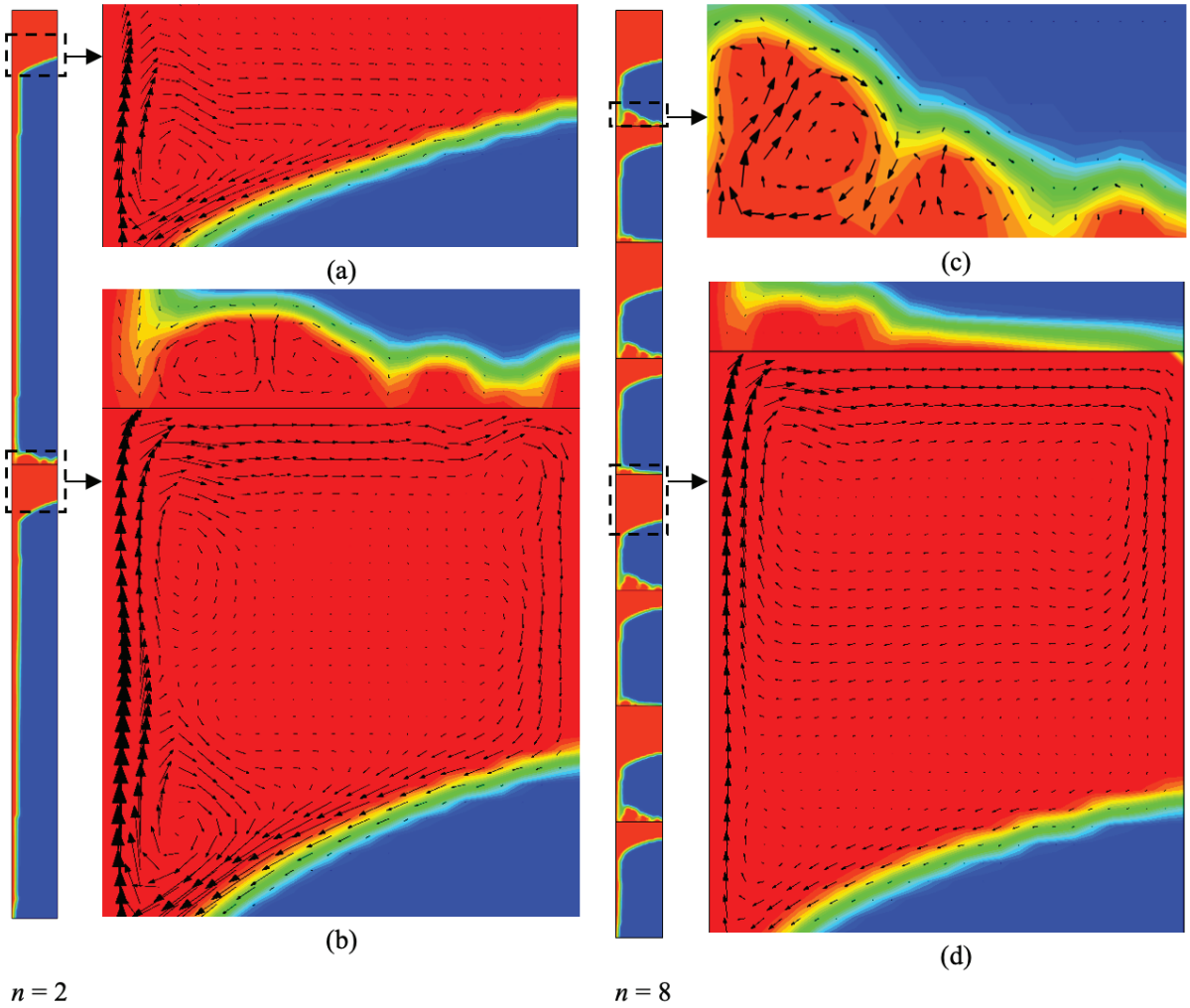


**Figure 7.** Velocity vector during melting of PCMs at $Re$ = 10000, $R/r$ = 3, $t$ = 0.25 hr.

compared to single-layer PCMs, the 8-layer alternating PCM arrangement uses more layers, creating a higher surface area for heat transfer. Having more surface area can expedite heat transport and minimize the overall melting time. Secondly, in the multi-layer arrangement heat is transported not only from the HTF to the PCM but also between the layers themselves. As the HTF moves along the walls, heat is absorbed by all PCM layers, which initiates the melting process and creates a melt pool in each layer. These melt pools create temperature gradients at the boundaries of each consecutive pair of PCMs, causing inter-layer heat transfer from the bottom to the higher layer due to temperature differences. The alternating arrangement of PCM-1 and PCM-2 is very useful because their different thermophysical properties, generate large variances in heat absorption capacities. These variations provide higher temperature gradients between consecutive layers, which increases the overall heat transfer rate of the system. As heat moves from a lower layer's melt pool to the higher layer, the temperature in the upper layer rises more quickly, facilitating faster melting. This inter-layer heat transfer process constantly generates favorable temperature gradients relative to the HTF, resulting in efficient heat distribution throughout the system. This ongoing process considerably increases the melting rate in multi-layered systems when compared to single-layer systems. As a result, the alternating PCM arrangement is superior to single-layer arrangements in terms of thermal storage performance, as it leverages the synergistic effects of different material properties to enhance heat absorption, storage, and heat transfer efficiency.

**During Solidification of PCM**

Figure 8a illustrates the time changes of the liquid fraction with the number of layers during the solidification process. It is observed that solidification becomes faster if the number of layers raises ($n$) from 2 to 8. It is seen that near the tube wall surface where the solidification process begins, spreading into PCM-1 and PCM-2. Figure 9

illustrates the liquid fraction and temperature contours that give a proper insight into the results. Notably, PCM-2 solidifies faster than PCM-1. The differences in solidification rates are due to a temperature gradient within the PCMs, which causes buoyancy-driven convection circulation within the melted PCMs. As seen in Figures 10a and 10b, velocity vectors reveal the formation of vortices within the PCMs. A single counter-rotating vortex forms within PCM-1, whereas multiple rotating vortices develop within PCM-2. The presence of multiple vortices in PCM-2 improves fluid mixing and promotes better convective heat circulation. As a result, PCM-2 dissipates heat more efficiently and achieves the solidus temperature faster than PCM-1. From Figure 9, it can be seen that at $n$ = 8, each layer solidifies and the overall solid fraction is greater than $n$ = 2. Firstly, with an increasing number of layers, there could be a higher number of nucleation sites available for phase transition. The increased surface area provided by additional layers can promote better heat transfer, which can enhance the solidification process. Secondly, during solidification, temperature gradients inside the melted PCMs cause buoyancy-driven flow patterns, which may result in the formation of vortices. These vortices have an important role in redistributing liquid material and promoting mixing, hence accelerating the solidification process. The alternating arrangement of PCM-1 and PCM-2 accentuates these occurrences. The creation of clockwise and counter-clockwise vortices within PCM-2 is particularly noteworthy. This unique occurrence can be due to the alternating arrangement, which causes disruptions in flow dynamics, resulting in the formation of diverse vortex patterns. Furthermore, inter-layer heat transfer between

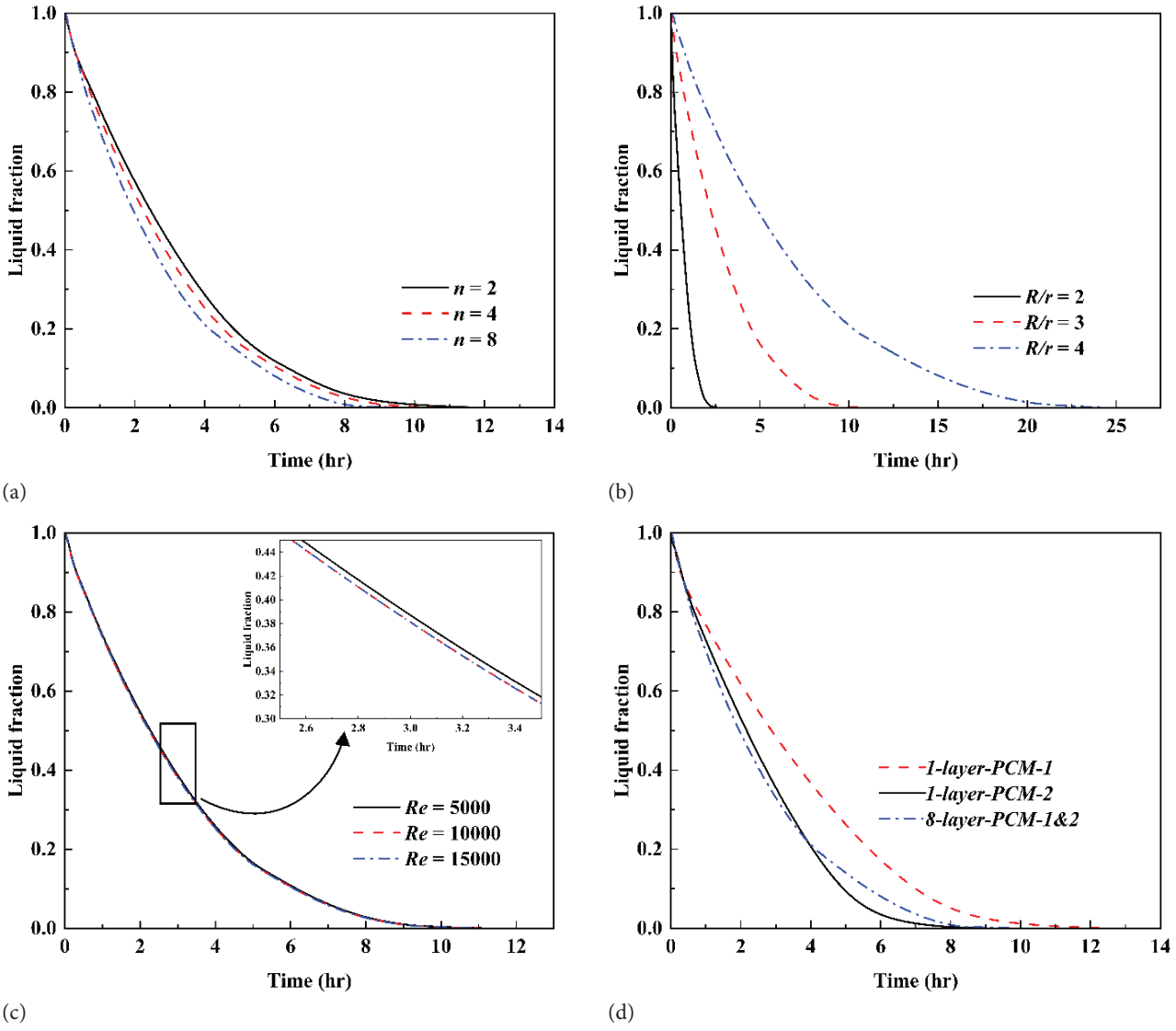


**Figure 8.** Temporal variation of liquid fraction with different parameters during solidification of PCMs at (a) $Re$ = 10000, $R/r$ = 3, (b) $Re$ = 10000, $n$ = 4, (c) $n$ = 4, $R/r$ = 3, (d) $Re$ = 10000, $R/r$ = 3.

the alternating layers of PCM-1 and PCM-2 aids in the generation of multiple vortices, as temperature gradients between successive layers cause buoyancy-driven flow patterns, promoting the emergence of complex flow structures. Figures 10c and 10d exhibit velocity vectors at $n = 8$, which depict flow mechanics in the PCM-1 and PCM-2 alternating arrangement. Notably, buoyancy-driven flow patterns are prominent in PCM-1, whereas PCM-2 leads to the formation of both clockwise and counter-clockwise vortices, which help to speed up solidification. The increase in the number of layers potentially enhances vortex formation as the liquid material traverses narrower interlayer spaces. This intensified flow creates more vortices, thereby further hastening the solidification process. This results in a reduction in the solidification time at about 19% if the number of layers increases from 2 to 8.

Figure 8b represents the time variation of the liquid fraction with the radius ratio of shell and tube. It is evident that increasing the *R/r* ratio and keeping the tube ratio constant leads to an increase in solidification time. The justification of such results can be explained in the context of thermal resistance, mass, and temperature gradient. The heat resistance of the liquid PCMs and the HTF increases as the *R/r* ratio rises while the tube ratio remains constant. With a larger shell diameter, heat must travel a greater distance through the shell before being released to the HTF, resulting in delayed solidification. The mass of the PCM also has an important influence. As PCMs cool and solidify, the mass of the solid PCMs increases while the mass of the liquid PCMs decreases. As the *R/r* ratio grows, so does the mass of the liquid PCMs in contact with the tube's cold surface. The surface-to-volume ratio decreases as the *R/r* ratio increases, slowing the conductive heat transfer rate. Furthermore, when the *R/r* ratio increases the shell radius increases, reducing the radial temperature gradient. This is because, as the radial distance increases, the heat transfer rate from the solidification front to the PCMs' outer surface decreases. As a result, the temperature gradient decreases and solidification occurs at a slower rate. Quantitatively, it is observed that if the *R/r* ratio is reduced from 4 to 2, the solidification rate improves to about 89%. On the contrary, the thermal storage capacity is reduced by the lower *R/r* ratio. So, it is important to take into account the impact of the radius ratio of the shell to the tube when constructing a thermal energy storage system, as it can have a substantial impact on the system's solidification time and

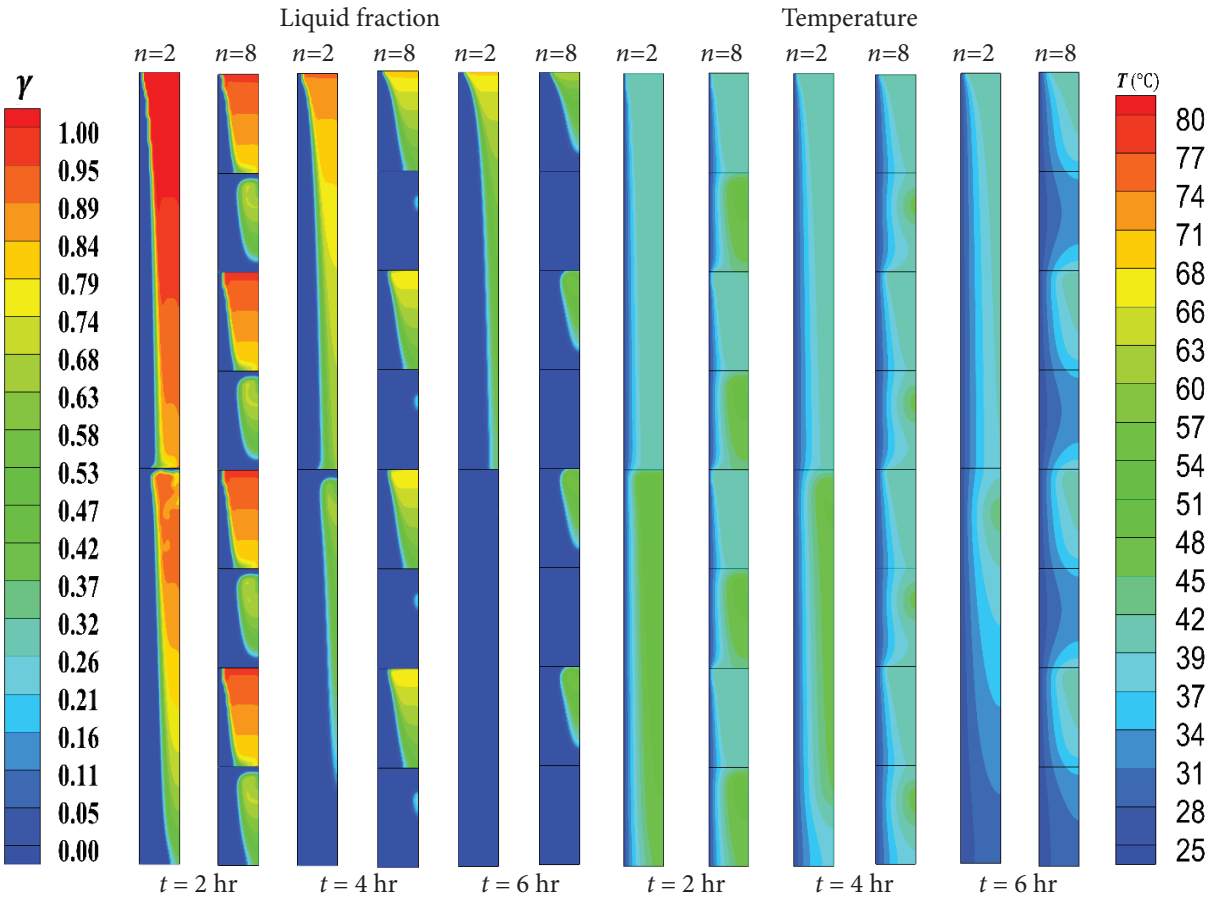


**Figure 9.** Contours of liquid fraction and temperature at different flow times and number of layers during solidification of PCMs at $Re = 10000$, $R/r = 3$.

overall performance. In such situations, such as in emergency backup power systems, the storage with a lower *R/r* ratio can quickly store and release large amounts of heat energy.

Figure 8c describes the variation of liquid fraction with Reynolds number, keeping all other parameters fixed. It can be seen that the solidification rate is dependent on the HTF flow Reynolds number. However, the changes due to the Reynolds number are less significant. When the Reynolds number rises, the efficiency of heat transport from the PCM to the HTF increases, which causes the liquid fraction of the PCMs to decrease during solidification. As the Reynolds number rises from *Re* = 5000 to *Re* = 10000, turbulence increases noticeably, which causes the liquid fraction of the PCM to noticeably decrease. However, the influence of turbulence on heat transfer becomes less significant as the Reynolds number rises from 10,000 to 15,000, while the liquid fraction of the PCMs remains mostly unchanged. This is because turbulence intensity and kinetic energy increase at very high Reynolds numbers, which may hinder solidification by causing fluctuations in temperature and flow velocity that may slow down the formation of a smooth and uniform solidification front. As a result, the effect of turbulence on the solidification rate normally reduces over a threshold Reynolds number. In addition, when the Reynolds number increases, the ability of HTF to remove heat from the PCMs is restricted by the conductive resistance of the PCMs themselves. This means that even though the HTF may be capable of removing heat more effectively, the rate at which the PCMs can transport this heat to the solidification front does not rise proportionally. The overall solidification time minimizes about 1% if the HTF Reynolds number increases from 5000 to 15000.

Figure 8d presents a comparative analysis of the time variation of liquid fraction during solidification across three different cases, namely, *1-layer-PCM-1*, *1-layer-PCM-2*, and *8-layer-PCM-1&2* alternately arranged configuration. Initially, the solidification rate appears to rise significantly in the 8-layer alternating arrangement as compared to the single-layer PCM-1 configuration. However, as compared to single-layer PCM-2, it is clear that the solidification rate in the 8-layer configuration begins to decline after 4 hours. The decline can be attributed to the dynamic interaction between thermal characteristics and phase transition kinetics. While PCM-2 initially solidifies rapidly due to its proximity to the solidification temperature, the subsequent presence of solid PCM-2 may act as an insulating barrier, preventing additional heat transfer to the remaining PCM-1

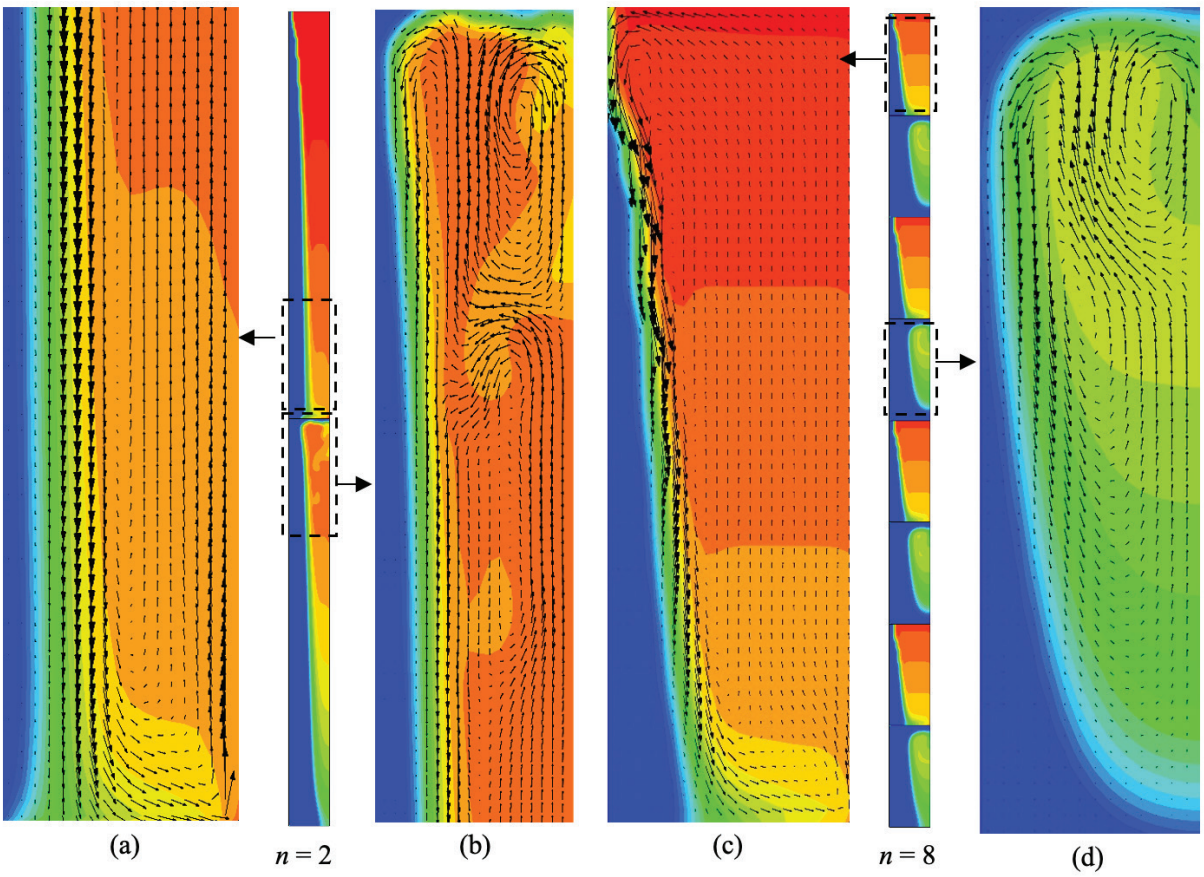


**Figure 10.** Velocity vector during solidification of PCMs at *Re*=10000, *R/r*=3, *t*=2 hr.

layers. From the liquid fraction contour depicted in Figure 9, it can be seen that after 4 hours, PCM-2 almost solidifies, leaving only PCM-1, causing the solidification rate to decline. Nevertheless, the complete solidification time in an 8-layer case is reduced approximately by 21.9% in comparison with a single-layer PCM-1. Therefore, the multi-layered arrangement of two PCMs alternating arrangement proves to be a more efficient way to reduce the overall solidification time while maintaining a reasonable solidification rate.

**Storage performance evaluation**

The evaluation of a heat storage system's performance stands essential for ensuring efficient storage and release of thermal energy. For evaluating the impact of all parameters on energy storage and retrieval performances, at a fixed time energy storage density has been calculated. Figure 11 represents the energy storage density with different parameters after 0.75hr completion of melting and solidification.

From Figure 11a, it is seen that at $t = 0.75$ hr, energy storage density is enhanced if the number of layers ($n$) increases from 2 to 8 during the melting process. In comparison with a 2-layer system, an 8-layer alternating arrangement can store 33.2% more energy at a fixed time. Besides, it can be also observed that at $t = 0.75$ hr, energy storage density is reduced if the layer increases from 2 to 8 during the solidification. It indicates that with the rise in the number of layers, more energy can be retrieved. In comparison with a 2-layer system, an 8-layer system can retrieve about 5.3% more energy at a fixed time. The key factors of these findings are applicable especially when quicker energy storage and retrieval is desired.

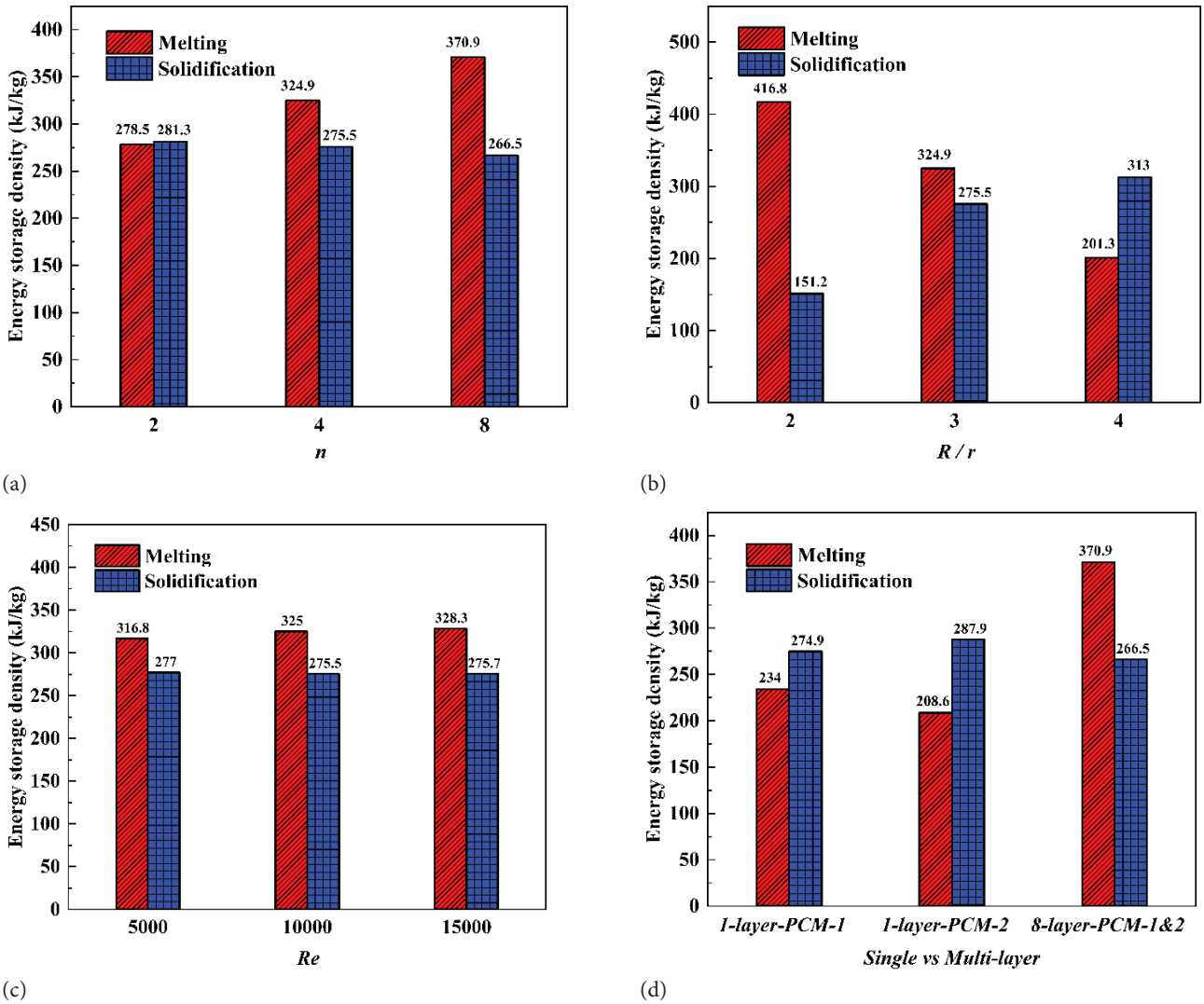


**Figure 11.** Quantitative performance evaluation of storage system based on energy storage density with different parameters after 0.75 hr completion of melting and solidification at (a) $Re = 10000$, $R/r = 3$, (b) $Re = 10000$, $n = 4$, (c) $n = 4$, $R/r = 3$, (d) $Re = 10000$, $R/r = 3$.

Figure 11b offers valuable insight into the storage performance of a system, particularly concerning the radius ratio of the shell to the tube at a specific time. Upon examination, it becomes apparent that the storage unit with a lower radius ratio is capable of efficiently storing the maximum amount of energy during the melting process, as compared to other storage units. The energy storage density tends to decrease as the radius ratio increases from 2 to 4. Based on quantitative analysis, it can be seen that the energy storage unit with $R/r = 2$ can store about 107% more energy than the one with $R/r = 4$, at a fixed time of $t = 0.75$hr. Besides, it can also be found that during the solidification process, a lower $R/r$ ratio-based storage system maximum energy can be retrieved quickly. Quantitatively, using a storage system having $R/r = 2$, 51.7% more energy can be retrieved quickly as compared to $R/r = 4$.

Figure 11c represents the energy storage and retrieval performance based on the HTF flow Reynolds number ($Re$) after 0.75hr completion on melting and solidification. The results of this study illustrate that during the melting process, increasing the Reynolds number of the flow from 5000 to 15000 leads to an increase in the energy storage density. Specifically, the data shows that there is 3.6% more energy that can be stored. Similarly, during the solidification process, at a higher Reynolds number more quickly energy can be retrieved. Quantitatively, 0.5% more energy can be retrieved during solidification. This study reveals that for quicker storage and removal of energy, the flow Reynolds number is also a vital factor that needs to be under consideration for the designing of energy storage systems.

Figure 11d presents a comparative analysis of the storage performance of three different cases, namely *1-layer-PCM-1*, *1-layer-PCM-2*, and *8-layer-PCM-1&2* alternating arrangement. The results indicate that after 0.75hr of melting, the 8-layer two PCM alternating arrangement can store significantly more energy compared to the single-layer individual cases. In quantitative terms, the 8-layer two PCM alternating arrangement can store approximately 58.5% and 77.8% more energy than the single-layer individual PCMs, respectively. Additionally, the study also reveals that during solidification, the 8-layer two PCM alternating arrangement can retrieve more energy than the individual cases. At a fixed time, the 8-layer two PCM alternating arrangement can retrieve energy at 3.1% and 7.4% more than the single-layer individual cases, respectively. Therefore, the results of the study suggest that using a multi-layered dual PCM alternating arrangement can improve energy storage and retrieval performance compared to using a single-layered PCM.

## CONCLUSION

In conclusion, this parametric study offers a range of benefits that make it a compelling choice for designing an efficient thermal energy storage system. This study reveals the effect of different design and flow parameters on the storage performances during both the melting and solidification of PCMs. This study also emphasized an insight comparison between single-layer PCM over multi-layered dual PCM alternating arrangement. The following are some key conclusions:

- As the number of layers ($n$) is increased from 2 to 8 the time required for complete melting and solidification time is reduced by about 44.3% and 19% respectively. In the context of energy storage/retrieval, an 8-layer system exhibits a capacity to store or release energy more rapidly compared to the 2-layer system with improvements of approximately 33.2% and 5.3% during the melting and solidification process respectively.
- If the radius ratio, $R/r$ decreases from 4 to 2, the overall melting and solidification time is reduced by about 78.6% and 89% respectively. Storage of $R/r = 2$ can store/release energy quicker than $R/r = 4$ at about 107% and 51.7% during the melting and solidification process respectively.
- The impact of HTF flow Reynolds number ($Re$) on melting and solidification is comparatively small. The rate of melting and solidification improves by about 5.8%. and 1% as the HTF flow Reynolds number raises from 5000 to 15000. The energy storage/retrieved density also advanced by about 3.6% and 0.5% as the flow Reynolds number increased.
- Finally, in comparison with *1-layer-PCM-1* and *1-layer-PCM-2*, *8-layer-PCM-1&2* alternating arrangement can augment melting and solidification rate. The total melting time decreases in the 8-layered configuration by 33.65% and 55.84% as compared to the single-layer of PCM-1 and PCM-2 respectively. Similarly, the complete solidification time is reduced by 21.9% compared to a single-layer PCM-1 case. Energy storage/retrieval performance advanced in an 8-layer system. It can store energy more rapidly about 58.5% and 77.8% compared to single-layer individual PCMs. Similarly, retrieval performances also accelerated by approximately 3.1% and 7.4% compared to single-layer individual PCMs.

In summary, multi-layer alternating PCM configurations ensure efficient operation, especially in applications where rapid energy storage/retrieval is crucial. This versatility makes them ideal for diverse applications, including renewable energy systems such as solar power plants, industrial processes, building HVAC systems, electronics, etc. Although this study shows improved melting and solidification performance adopting multi-layer twin PCMs in alternately arranged manners, multiple PCMs in the multi-layer arrangement need to be studied further. The arrangement of PCMs is also to be a major factor for study. The optimization of different parameters on the maximization of energy storage and retrieval performance needs to be extended further.

## NOMENCLATURE

**Abbreviation**

| | |
|---|---|
| PCM | Phase change material |
| HTF | Heat transfer fluid |

| | |
|---|---|
| LHTES | Latent heat thermal energy storage |
| TES | Thermal energy storage |

**List of symbols**

| | |
|---|---|
| $C_{mush}$ | Mushy zone constant [kg/ (m$^3$ s)] |
| $Cp$ | Specific heat [J/ (kg K)] |
| $Cp,v$ | PCM variable specific heat [J/ (kg K)] |
| $g$ | Acceleration due to gravity [m/s$^2$] |
| $h$ | Enthalpy [J/kg] |
| $K$ | Thermal conductivity [W/ (m K)] |
| $k$ | Turbulent kinetic energy [J] |
| $L$ | Latent heat of fusion [J/kg] |
| $m$ | Mass [kg] |
| $n$ | Number of layers |
| $r$ | Radius of tube |
| $R$ | Radius of shell |
| $Re$ | Reynolds number |
| $t$ | Time [hr] |
| $T$ | Temperature [°C] |
| $\vec{V}$ | Velocity vector [m/s] |
| $V$ | Volume [m$^3$] |
| $x$ | Radial coordinate |
| $z$ | Axial coordinate |
| $K_t$ | Thermal conductivity due to turbulence [W/ (m K)] |

***Greeks***

| | |
|---|---|
| $\gamma$ | Liquid fraction |
| $\varepsilon$ | Turbulent K.E. dissipation rate [m$^2$ /s$^3$] |
| $\mu$ | Dynamic viscosity [kg/ (m s)] |
| $\mu_t$ | Turbulent viscosity [kg/ (m s)] |
| $\rho$ | Density [Kg / m$^3$] |

## ACKNOWLEDGMENTS

The authors would like to convey their sincere gratitude to the Ministry of Education, Government of India, for generously providing financial support in the form of a Ph.D. fellowship during this research.

## AUTHORSHIP CONTRIBUTIONS

Authors equally contributed to this work.

## DATA AVAILABILITY STATEMENT

The authors confirm that the data that supports the findings of this study are available within the article. Raw data that support the finding of this study are available from the corresponding author, upon reasonable request.

## CONFLICT OF INTEREST

The author declared no potential conflicts of interest with respect to the research, authorship, and/or publication of this article.

## ETHICS

There are no ethical issues with the publication of this manuscript.

## STATEMENT ON THE USE OF ARTIFICIAL INTELLIGENCE

Artificial intelligence was not used in the preparation of the article.

## REFERENCES

[1] Korti AIN. Numerical simulation on the effect of latent heat thermal energy storage unit. J Therm Eng 2016;2:599-607. [Crossref]

[2] Benbrika M, Teggar M, Benbelhout M. Effect of orientation of elliptic tube on the total melting time of latent thermal energy storage systems. J Therm Eng 2021;7:1479-1488. [Crossref]

[3] Patil R, Desai A. Performance of phase changing material in an artificially created cold region to promote latent heat thermal energy storage. J Therm Eng 2021;7:1694-1703. [Crossref]

[4] Aljabair S, Alesbe I, Ibrahim SH. Review on latent thermal energy storage using phase change material. J Therm Eng 2023;9:247-256. [Crossref]

[5] Elfeky KE, Ahmed N, Wang Q. Numerical comparison between single PCM and multi-stage PCM based high temperature thermal energy storage for CSP tower plants. Appl Therm Eng 2018;139:609-622. [Crossref]

[6] Prieto C, Cabeza LF. Thermal energy storage (TES) with phase change materials (PCM) in solar power plants (CSP). Concept and plant performance. Appl Energy 2019;254:113646. [Crossref]

[7] Gurupatham SK, Manikandan GK, Fahad F. Harnessing and storing solar thermal energy using phase change material (pcm) in a small flat plate collector. J Therm Eng 2020;6:511-520. [Crossref]

[8] Ben Zohra M, Riad A, Alhamany A, Sennoune M, Mansouri M. Improvement of thermal energy storage by integrating pcm into solar system. J Therm Eng 2020;6:816-828. [Crossref]

[9] Kumar AR, Ramakrishnan M. A scoping review on recent advancements in domestic applications of solar thermal systems. J Therm Eng 2022;8:426-444. [Crossref]

[10] Azeez K, Ahmed Ri, Obaid Za, Azzawi Idj. Heat transfer enhancement and applications of thermal energy storage techniques on solar air collectors: A review. J Therm Eng 2023;9:1356-1371. [Crossref]

[11] Nwosu Ec, Nsofor K, Nwaji Gn, Ononogbo C, Ofong I, Ogueke N V., et al. Extended experimental investigation of a double-effect active solar still with a paraffin wax, in Owerri, Nigeria. J Therm Eng 2023;9:1189-1207. [Crossref]

[12] Rastogi M, Chauhan A, Vaish R, Kishan A. Selection and performance assessment of Phase Change Materials for heating, ventilation and air-conditioning applications. Energy Convers Manag 2015;89:260-269. [Crossref]
[13] Ljungdahl V, Taha K, Dallaire J, Kieseritzky E, Pawelz F, Jradi M, et al. Phase change material based ventilation module-Numerical study and experimental validation of serial design. Energy 2021;234:121209. [Crossref]
[14] Ismail M, Zahra WK, Ookawara S, Hassan H. Enhancing the Air Conditioning Unit Performance via Energy Storage of Different Inorganic Phase Change Materials with Hybrid Nanoparticles. JOM 2023:1-15. [Crossref]
[15] Bahrami L, Kasaeian A, Pourfayaz F, Ghafarian S. Modeling of the effect of nano-enhanced phase change material on the performance of a large-scale wallboard. J Therm Eng 2021;7:1857-1871. [Crossref]
[16] Kladisios P, Stegou-Sagia A. Using phase change materials in photovoltaic systems for cell temperature reduction: A finite difference simulation method. J Therm Eng 2016;2:897-906. [Crossref]
[17] Ali HM, Arshad A, Jabbal M, Verdin PG. Thermal management of electronics devices with PCMs filled pin-fin heat sinks: A comparison. Int J Heat Mass Transf 2018;117:1199-1204. [Crossref]
[18] Bondareva NS, Sheremet MA. Numerical simulation of natural convection melting in 2D and 3D enclosures. J Therm Eng 2019;5:51-61. [Crossref]
[19] Ren Q, Guo P, Zhu J. Thermal management of electronic devices using pin-fin based cascade microencapsulated PCM/expanded graphite composite. Int J Heat Mass Transf 2020;149:1-16. [Crossref]
[20] Ramesh KN, Sharma TK. Thermal analysis of PCM-based hybrid micro-channel heat sinks: A numerical study. J Therm Eng 2023;9:1015-1025. [Crossref]
[21] Merlin K, Soto J, Delaunay D, Traonvouez L. Industrial waste heat recovery using an enhanced conductivity latent heat thermal energy storage. Appl Energy 2016;183:491-503. [Crossref]
[22] Yazdani MR, Laitinen A, Helaakoski V, Farnas LK, Kukko K, Saari K, et al. Efficient storage and recovery of waste heat by phase change material embedded within additively manufactured grid heat exchangers. Int J Heat Mass Transf 2021;181:121846. [Crossref]
[23] Yadav C, Sahoo RR. Thermal analysis comparison of nano-additive PCM-based engine waste heat recovery thermal storage systems: an experimental study. J Therm Anal Calorim 2022;147:2785-802. [Crossref]
[24] Humphries WR. Performance of finned thermal capacitors. 1974.
[25] Swanson TD, Birur GC. NASA thermal control technologies for robotic spacecraft. Appl Therm Eng 2003;23:1055-1065. [Crossref]
[26] Agyenim F, Hewitt N, Eames P, Smyth M. A review of materials, heat transfer and phase change problem formulation for latent heat thermal energy storage systems (LHTESS). Renew Sustain Energy Rev 2010;14:615-628. [Crossref]
[27] Baghaei Oskouei S, Bayer Ö. Performance improvement in a vertical latent thermal energy storage tank with crossing heat transfer tubes. J Energy Storage 2024;88. [Crossref]
[28] Chaabane M, Mhiri H, Bournot P. Thermal performance of an integrated collector storage solar water heater (ICSSWH) with phase change materials (PCM). Energy Convers Manag 2014;78:897-903. [Crossref]
[29] Cano D, Funéz C, Rodriguez L, Valverde JL, Sanchez-Silva L. Experimental investigation of a thermal storage system using phase change materials. Appl Therm Eng 2016;107:264-270. [Crossref]
[30] Elbahjaoui R, El Qarnia H. Thermal performance of a solar latent heat storage unit using rectangular slabs of phase change material for domestic water heating purposes. Energy Build 2019;182:111-130. [Crossref]
[31] Şimşek F, Demirci H. Investigation of the use of new fin on the melting time of the phase change material stored in the heat exchanger by computational fluid dynamics analysis. J Build Eng 2024;91:109505. [Crossref]
[32] Trp A. An experimental and numerical investigation of heat transfer during technical grade paraffin melting and solidification in a shell-and-tube latent thermal energy storage unit. Sol Energy 2005;79:648-660. [Crossref]
[33] Zhang S, Pu L, Xu L, Liu R, Li Y. Melting performance analysis of phase change materials in different finned thermal energy storage. Appl Therm Eng 2020;176. [Crossref]
[34] Feng L, Liu J, Lu H, Chen Y, Wu S. A parametric study on the efficiency of a solar evacuated tube collector using phase change materials: A transient simulation. Renew Energy 2022;199:745-758. [Crossref]
[35] Alshihmani H, Maghrebi MJ, Sardarabadi M. Thermal performance prediction of a phase change material based heat-sink cooling system for a printed circuit board, using response surface method. J Energy Storage 2022;55:105499. [Crossref]
[36] Refaey HA, Abdo S, Saidani-Scott H, El-Shekeil YA, Bendoukha S, Barhoumi N, et al. Thermal regulation of photovoltaic panels using PCM with multiple fins configuration: Experimental study with analysis. Therm Sci Eng Prog 2024:102457. [Crossref]
[37] Xu H, Wang N, Zhang C, Qu Z, Cao M. Optimization on the melting performance of triplex-layer PCMs in a horizontal finned shell and tube thermal energy storage unit. Appl Therm Eng 2020;176:115409. [Crossref]

[38] Mebarek-Oudina F, Chabani I. Review on Nano Enhanced PCMs: Insight on nePCM Application in Thermal Management/Storage Systems. Energies 2023;16:1066. [Crossref]
[39] Li Z-R, Hu N, Fan L-W. Nanocomposite phase change materials for high-performance thermal energy storage: A critical review. Energy Storage Mater 2023;55:727-753. [Crossref]
[40] Sathishkumar A, Sundaram P, Cheralathan M, Kumar PG. Effect of nano-enhanced phase change materials on performance of cool thermal energy storage system: A review. J Energy Storage 2024;78:110079. [Crossref]
[41] Wang Q, Yang L, Song J. Preparation, thermal conductivity, and applications of nano-enhanced phase change materials (NEPCMs) in solar heat collection: A review. J Energy Storage 2023;63:107047. [Crossref]
[42] Maghrabie HM, Elsaid K, Sayed ET, Radwan A, Abo-Khalil AG, Rezk H, et al. Phase change materials based on nanoparticles for enhancing the performance of solar photovoltaic panels: A review. J Energy Storage 2022;48:103937. [Crossref]
[43] Bhutto YA, Pandey AK, Saidur R, Sharma K, Tyagi V V. Critical insights and recent updates on passive battery thermal management system integrated with nano-enhanced phase change materials. Mater Today Sustain 2023;23:100443. [Crossref]
[44] Algarni S, Mellouli S, Alqahtani T, Almutairi K, Khan A, Anqi A. Experimental investigation of an evacuated tube solar collector incorporating nano-enhanced PCM as a thermal booster. Appl Therm Eng 2020;180:115831. [Crossref]
[45] Bashirpour-Bonab H. Investigation and optimization of PCM melting with nanoparticle in a multi-tube thermal energy storage system. Case Stud Therm Eng 2021;28:101643. [Crossref]
[46] Elarem R, Alqahtani T, Mellouli S, Aich W, Ben Khedher N, Kolsi L, et al. Numerical study of an Evacuated Tube Solar Collector incorporating a Nano-PCM as a latent heat storage system. Case Stud Therm Eng 2021;24:100859. [Crossref]
[47] Rothan YA. Freezing process modeling within a cold storage tank with implement of nanoparticles. J Energy Storage 2024;88:111501. [Crossref]
[48] Zahid I, Farhan M, Farooq M, Asim M, Imran M. Experimental investigation for thermal performance enhancement of various heat sinks using Al2O3NePCM for cooling of electronic devices. Case Stud Therm Eng 2023;41:102553. [Crossref]
[49] Swamy KA, Verma S, Bhattacharyya S. Experimental and numerical investigation of nanoparticle assisted PCM-based battery thermal management system. J Therm Anal Calorim 2024. [Crossref]
[50] Cao Y, Faghri A. Performance characteristics of a thermal energy storage module: a transient PCM/forced convection conjugate analysis. Int J Heat Mass Transf 1991;34:93-101. [Crossref]
[51] Ismail KAR, Melo CA. Convection-based model for a PCM vertical storage unit. Int J Energy Res 1998;22:1249-1265. [Crossref]
[52] Trp A, Lenic K, Frankovic B. Analysis of the influence of operating conditions and geometric parameters on heat transfer in water-paraffin shell-and-tube latent thermal energy storage unit. Appl Therm Eng 2006;26:1830-1839. [Crossref]
[53] Tao Y-B, Li M-J, He Y-L, Tao W-Q. Effects of parameters on performance of high temperature molten salt latent heat storage unit. Appl Therm Eng 2014;72:48-55. [Crossref]
[54] Zheng Z-J, Xu Y, Li M-J. Eccentricity optimization of a horizontal shell-and-tube latent-heat thermal energy storage unit based on melting and melting-solidifying performance. Appl Energy 2018;220:447-454. [Crossref]
[55] Shen G, Wang X, Chan A, Cao F, Yin X. Investigation on optimal shell-to-tube radius ratio of a vertical shell-and-tube latent heat energy storage system. Sol Energy 2020;211:732-743. [Crossref]
[56] Vyshak NR, Jilani G. Numerical analysis of latent heat thermal energy storage system. Energy Convers Manag 2007;48:2161-2168. [Crossref]
[57] Akgün M, Ayd\in O, Kaygusuz K. Thermal energy storage performance of paraffin in a novel tube-in-shell system. Appl Therm Eng 2008;28:405-413. [Crossref]
[58] Seddegh S, Tehrani SSM, Wang X, Cao F, Taylor RA. Comparison of heat transfer between cylindrical and conical vertical shell-and-tube latent heat thermal energy storage systems. Appl Therm Eng 2018;130:1349-1362. [Crossref]
[59] Alaraji A, Alhussein H, Asadi Z, Ganji DD. Investigation of heat energy storage of RT26 organic materials in circular and elliptical heat exchangers in melting and solidification process. Case Stud Therm Eng 2021;28:101432. [Crossref]
[60] Dukhan WA, Dhaidan NS, Al-Hattab TA, Al-Mousawi FN. Phase-change of paraffin inside heat exchangers: an experimental study. Int J Environ Sci Technol 2022;19:3155-164. [Crossref]
[61] Zauglanmics E, Demircan T, Gemiciouglu B. Thermal analysis of phase changing material in heat exchanger. Arab J Sci Eng 2022:1-15.
[62] Paria S, Baradaran S, Amiri A, Sarhan AAD, Kazi SN. Performance evaluation of latent heat energy storage in horizontal shell-and-finned tube for solar application. J Therm Anal Calorim 2016;123:1371-1381. [Crossref]
[63] Joshi V, Rathod MK. Constructal enhancement of thermal transport in latent heat storage systems assisted with fins. Int J Therm Sci 2019;145:105984. [Crossref]
[64] Nakhchi ME, Esfahani JA. Improving the melting performance of PCM thermal energy storage with novel stepped fins. J Energy Storage 2020;30:101424. [Crossref]

[65] Nie C, Deng S, Liu J. Effects of fins arrangement and parameters on the consecutive melting and solidification of PCM in a latent heat storage unit. J Energy Storage 2020;29:101319. [Crossref]
[66] Nóbrega CRES, Ismail KAR, Lino FAM. Solidification around axial finned tube submersed in PCM: Modeling and experiments. J Energy Storage 2020;29:101438. [Crossref]
[67] Tiari S, Hockins A, Mahdavi M. Numerical study of a latent heat thermal energy storage system enhanced by varying fin configurations. Case Stud Therm Eng 2021;25:100999. [Crossref]
[68] Brousseau P, Lacroix M. Study of the thermal performance of a multi-layer PCM storage unit. Energy Convers Manag 1996;37:599-609. [Crossref]
[69] Li YQ, He YL, Song HJ, Xu C, Wang WW. Numerical analysis and parameters optimization of shell-and-tube heat storage unit using three phase change materials. Renew Energy 2013;59:92-99. [Crossref]
[70] Ezra M, Kozak Y, Dubovsky V, Ziskind G. Analysis and optimization of melting temperature span for a multiple-PCM latent heat thermal energy storage unit. Appl Therm Eng 2016;93:315-329. [Crossref]
[71] Beemkumar N, Karthikeyan A, Yuvarajan D, Lakshmi Sankar S. Experimental Investigation on Improving the Heat Transfer of Cascaded Thermal Storage System Using Different Fins. Arab J Sci Eng (Springer Sci Bus Media BV) 2017;42. [Crossref]
[72] Sunku Prasad J, Muthukumar P, Anandalakshmi R, Niyas H. Comparative study of phase change phenomenon in high temperature cascade latent heat energy storage system using conduction and conduction-convection models. Sol Energy 2018;176:627-637. [Crossref]
[73] Kareem BE, Adham AM, Yaqob BN. Design and Optimization of Air to PCM Heat Exchanger Using CFD. Arab J Sci Eng 2022:1-15. [Crossref]
[74] Rubitherm Technologies GmbH. RT- LINE Data Sheet 2020.
[75] Brent AD, Voller VR, Reid KJ. Enthalpy-Porosity Technique For Modeling Convection-Diffusion Phase Change: Application To The Melting Of A Pure Metal. Numer Heat Transf 1988;13:297-318. [Crossref]
[76] Zhang D, Zhang F, Tang S, Guo C, Qin X. Performance evaluation of cascaded storage system with multiple phase change materials. Appl Therm Eng 2021;185:116384. [Crossref]

## APPENDIX

The Finite Volume Method (FVM) is a key technique in computational fluid dynamics (CFD), and it is especially relevant to our research on thermal energy storage systems due to its multiple benefits. These benefits include conservation properties, grid flexibility, conservative interpolation, consistent stencils, physics adaptation, stability, precision, parallelizability, and strong commercial support from ANSYS Fluent. The advantages of the Finite Volume Method (FVM) and the FVM simulation steps are illustrated in the flow chart in Figure 12.

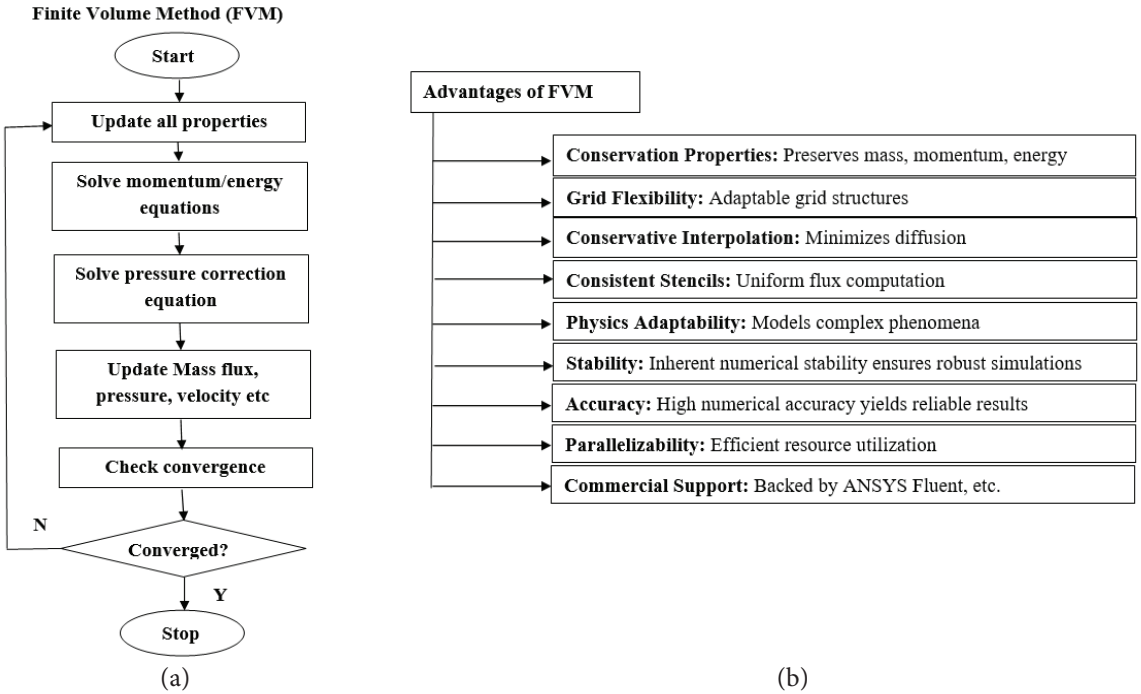


**Figure 12.** Flow chart of Finite Volume Method (FVM) (a) steps, (b) advantages